ELSEVIER

Physica C 233 (1994) 367–372

PHYSICA C

Magnetic properties of YNi_2B_2C superconductor

R. Prozorov [a,*], E.R. Yacoby [a], I. Felner [b], Y. Yeshurun [a]

[a] *Department of Physics, Bar-Ilan University, 52900 Ramat-Gan, Israel*
[b] *Racah Institute of Physics, The Hebrew University, Jerusalem, Israel*

Received 19 August 1994; revised manuscript received 8 September 1994

Abstract

We report on a study of the magnetic properties of the intermetallic superconductor YNi_2B_2C in a wide range of magnetic fields (up to 8 T) and temperatures (4.4–16 K). The results yield the characteristic length scales and fields for this compound: $\lambda(0) \approx (3.5 \pm 0.5) \times 10^{-5}$ cm, $\xi(0) \approx (10 \pm 2) \times 10^{-7}$ cm, $H_{c1}(0) \approx 83$ G and $H_{c2}(0) \approx 47600$ G. We compare our results with those obtained by other groups and add new information on thermodynamic properties, in particular on the lower critical field, and on *irreversible* magnetic features such as the critical current, pinning force and magnetic relaxation. We conclude that YNi_2B_2C is a type-II superconductor with relatively weak pinning centers.

1. Introduction

The intensive activity in intermetallic superconducting (SC) phases has slowed down during the last decade. In particular, no new families with high T_c have been discovered since the 1973 report on A15 Nb_3Ge with a transition temperature $T_c = 23.2$ K [1]. Recently, however, a small fraction (about 2%) of a SC phase ($T_c = 12$ K) was detected in samples of nominal composition YNi_4B [2]. Subsequently, the SC volume fraction was significantly enhanced by adding small amounts of C and $T_c = 15$ K was reported in a multiphase $YNi_4BC_{0.2}$ sample [3]. Superconducting single-phase novel Ni-compounds with the composition RNi_2B_2C (R = rare-earth) have been established by Cava et al. [4] where the highest T_c, 15.6 and 16.6 K, were observed for R = Y and Lu, respectively. Several $YNi_4BC_{0.2}$ samples prepared in our laboratory did not show SC, and we have concluded that SC in this phase [3] is due to an impurity phase of the tetragonal YNi_2B_2C phase [5].

The new quaternary RNi_2B_2C compounds crystallize in the well known tetragonal $ThCr_2Si_2$-type structure (space group I4/mmm). The nickel boride framework of this structure is modified by the insertion of a carbon atom in the R layer where alternating layers of Ni_2B_2 and RC exist [4]. It has been widely speculated that the low mass of the boron is conducive to the occurrence of high phonon frequencies and consequently to high T_c. It seems likely that the relatively high T_c is due to the three-dimensional nature of the bonding associated with this structure, whereas the quite substantial contraction (compared to YNi_2B_2) of the a lattice parameter indicates strong Ni–B bonds in the Ni_2B_2 planes. The role of carbon in this system is not yet known.

The main goal of this paper is to characterize the magnetic properties of YNi_2B_2C. We report here on magnetic measurements from which we evaluate the lower critical field H_{c1}, the upper critical field H_{c2}, the irreversibility field H_{irr}, the Ginzburg–Landau parameter κ, the penetration depth λ and the coher-

* Corresponding author.

SSDI 0921-4534(94)00595-8

ence length ξ. We compare our results with previous reports on the magnetic properties of YNi_2B_2C [6–8] and add some new information on the lower critical field. Special attention is given to the irreversible properties of YNi_2B_2C – critical current, scaling of the pinning force and the relaxation.

2. Experimental

YNi_2B_2C was prepared by melting of high purity constituents in an induction furnace under argon atmosphere. The ingot was annealed at 950°C for several days and the X-ray diffraction pattern indicates that the sample is nearly single phase. Impurity peaks were smaller than 3%. The lattice parameters $a=3.524$ [1] and $c=10.535$ [2] Å are in agreement with the literature [4]. Two pieces, (139.4 and 290.2 mg), were cut from the ingot. These pieces are denoted below as sample #1 and sample #2, respectively. The SC transition $T_c=15.5$ K [1] for these samples was measured by a SQUID magnetometer at 10 G.

We used an Oxford-Instrument Vibrating Sample Magnetometer (VSM) for high-field (up to 5 T) measurements and a Quantum Design SQUID for the low-field region (up to 350 G).

3. Results

The low-field part of the magnetization loops (after zero-field cooling) of sample #1, measured by SQUID at $T=5$, 7, 9, 11, 13 and 14.5 K, are shown in Fig. 1. Fig. 2 shows a typical set of magnetization loops of sample #2 measured by VSM at $T=4.4$, 7, 9 K. Both the irreversible (M_{irr}) and the reversible (M_{rev}) moments can be deduced from the ascending ($M\uparrow$) and descending ($M\downarrow$) branches of the magnetization loop. Apparently, the irreversible moment $M_{irr}=|M\uparrow-M\downarrow|$ is comparable and even less than the reversible magnetization $M_{rev}=\frac{1}{2}|M\uparrow+M\downarrow|$. This implies rather weak pinning in our YNi_2B_2C compound. The inset in Fig. 2 exhibits typical data, at $T=5$ K, up to magnetic field 5 T.

Below we extract from the magnetization loops information on the critical fields and characteristic length scales of YNi_2B_2C in the superconducting state.

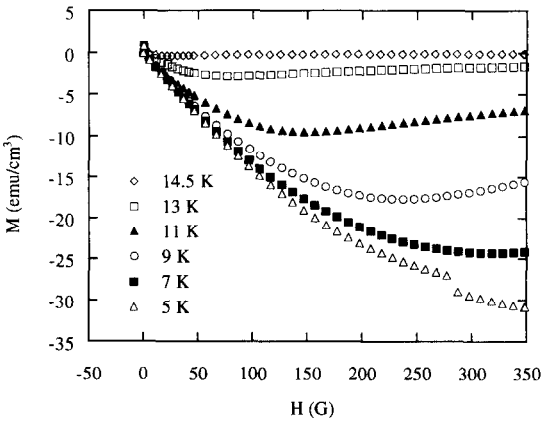

Fig. 1. Low-field data of the magnetization curves measured at $T=5$, 7, 9, 11, 13 and 14.5 K.

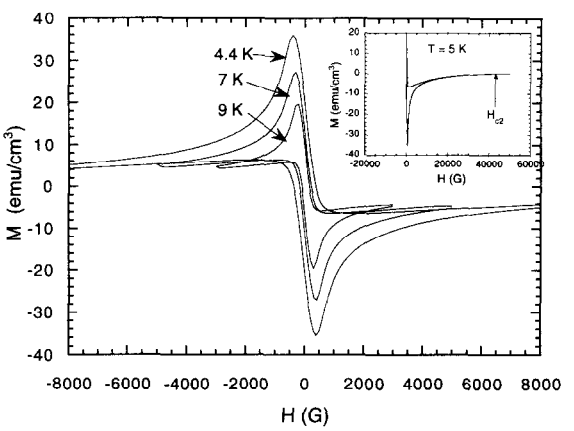

Fig. 2. Magnetization loops at $T=4.4$, 7 and 9 K measured by VSM. (Insert) high-field magnetization loop at $T=5$ K.

3.1. Lower critical field H_{c1}

In the Meissner state the total magnetic moment of a superconductor is given by (see e.g. Ref. [9]) $M=-H_aV/4\pi(1-N)$, where H_a is the external magnetic field, V is the volume of a sample, and N is the demagnetizing factor. We have found experimentally that $N\approx 0.4$. For accurate determination of the deviation from the linear behavior we have used the parameter $p=4\pi M/H_aV=-1/(1-N)$, which is constant up to the applied field H_{c1}^a. We use here the superscript to denote the applied field, before the correction for demagnetization. In Fig. 3 the parameter p is plotted as a function of the external magnetic field at various temperatures. Using $\Delta p\approx 0.05$ as a

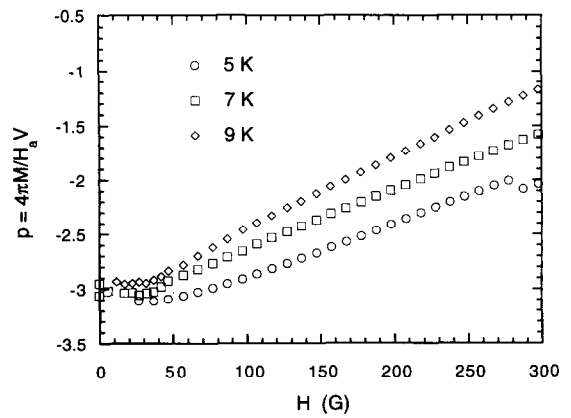

Fig. 3. The parameter $p=4\pi M/H^0V=-1/(1-N)$ vs. the magnetic field at $T=5$, 7 and 9 K.

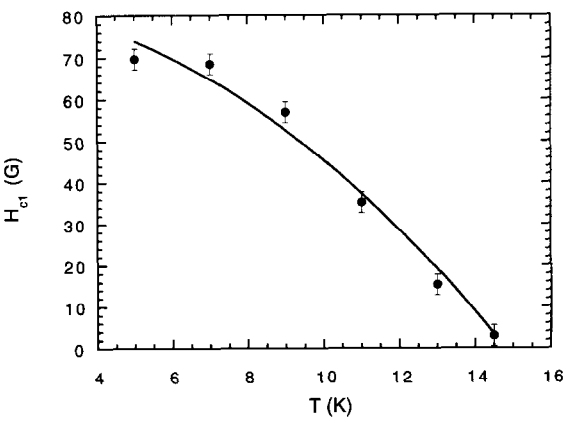

Fig. 4. The lower critical field H_{c1} vs. temperature.

criterion for deviation from a constant value, we obtain the lower critical field $H^a_{c1}(T)$ within an error $\Delta H^a_{c1}\approx 5$ G. The actual values of $H_{c1}=H^0_{c1}/(1-N)$, are shown in Fig. 4. The symbols are the experimental points and the solid line is a fit to the empirical equation $H_{c1}(T)=H_{c1}(0)[1-(T/T_c)^2]$ with $H_{c1}(0)=83.5\pm 2.5$ G. We note that our determination of the lower critical field is an upper estimation for H_{c1} due to possible effects of surface barriers.

3.2. Upper critical field H_{c2}

The upper critical field H_{c2} was identified as the onset of a diamagnetic signal during the decrease of the magnetic field from 8 T. Above H_{c2} there was no diamagnetic signal within the resolution of VSM (10^{-5} emu). For the onset we used the criterion $M=0.005$ emu; this yields the upper critical field with an accuracy of approximately ± 1000 G. In Fig. 5 open circles show our estimation for the upper critical field. The data in the figure follow the same functional form as for the lower critical field, namely $H_{c2}(T)=H_{c2}(0)[1-(T/T_c)^2]$ with $H_{c2}(0)\approx 47600\pm 1000$ G. This is shown by the solid line in Fig. 5.

3.3. Irreversibility field $H_{irr}(T)$

The irreversibility field was determined as the field at which the difference between the ascending and descending branches of the magnetization loop exceeded $\Delta M\approx 0.005$ emu. This gives an accuracy of about $\Delta H_{irr}\approx 1000$ G. The irreversibility field $H_{irr}(T)$ for sample #2 is shown in Fig. 5 by open squares. The solid line is a fit by $H_{irr}(T)=H_{irr}(0)(1-T/T_c)^{2.7}$ with $H_{irr}(0)\approx 81000\pm 500$ G. The value for $H_{irr}(0)$ has no direct physical meaning; it simply characterizes the general behavior of $H_{irr}(T)$. The fact that $H_{irr}(0)\gg H_{c2}(0)$ means that the equation $H_{irr}(T)=H_{irr}(0)(1-t)^{2.7}$ is not valid at low temperatures.

3.4. Coherence length $\xi(T)$ and penetration length $\lambda(T)$

By combining two well known formulae [10],

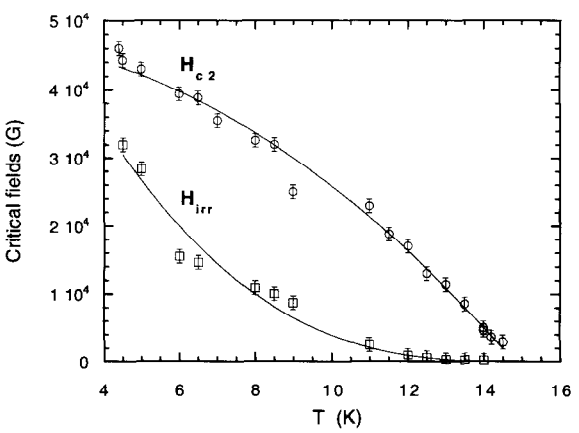

Fig. 5. The upper critical field $H_{c2}(T)$ and the irreversibility field $H_{irr}(T)$.

$$H_{c1} = \frac{\phi_0}{4\pi\lambda^2}\,[\ln(\kappa)+0.5]\,, \tag{1a}$$

where $\phi_0 \approx 2.0679\times10^{-7}$ G cm^2 is a flux quantum, $\kappa=\lambda/\xi$ is the Ginzburg–Landau parameter, and

$$H_{c2} = \frac{\phi_0}{2\pi\xi^2}\,, \tag{1b}$$

we arrive at the useful relationship:

$$2\frac{H_{c1}}{H_{c2}} = \frac{\ln(\kappa)+0.5}{\kappa^2}\,. \tag{2}$$

To get κ we solved Eq. (2) numerically for each of the experimental critical fields (i.e. for different temperatures). The parameter κ appears to be temperature independent, $\kappa \approx 35 \pm 3$.

The characteristic length scales for YNi_2B_2C were evaluated from $H_{c1}(T)$ and $H_{c2}(T)$ by using

$$\xi(T) = \sqrt{\frac{\phi_0}{2\pi H_{c2}(T)}} \tag{3a}$$

and

$$\lambda(T) = \kappa\xi(T)\,. \tag{3b}$$

The resulting curves are presented in Fig. 6. Both can be fitted in the whole temperature range using the well known relation $l(T) = l(0)\sqrt{1-(T/T_c)^4}$, where l is either λ or ξ. Zero-temperature values for characteristic length scales are $\lambda(0) \approx (3.5\pm0.5)\times10^{-5}$ cm and $\xi(0) \approx (1\pm0.2)\times10^{-6}$ cm.

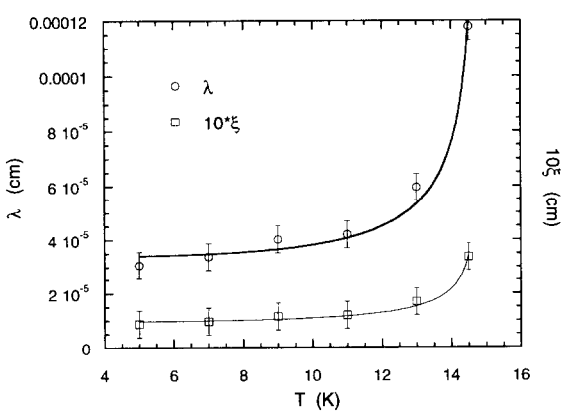

Fig. 6. The characteristic lengths $\lambda(T)$ and $\xi(T)$.

3.5. Comparison with previous results

Several groups [6–8] have reported on magnetic measurements in YNi_2B_2C. We compare their results with ours in Figs. 7 and 8. As can be seen, both H_{c2} and H_{irr} are in agreement with previous works, Refs. [6,7]. We note that in Ref. [6] a single YNi_2B_2C crystal was measured ($H\|c$), and this may explain the discrepancy in the data for H_{c2}. Concerning H_{c1}, we are aware of only one data point $H_{c1}(5\text{ K}) \approx 300$ G from Ref. [8]; this value is an order of magnitude higher than ours.

3.6. Critical current and the pinning force

One of the important characteristics of type-II superconductors is the pinning force density [9–11]

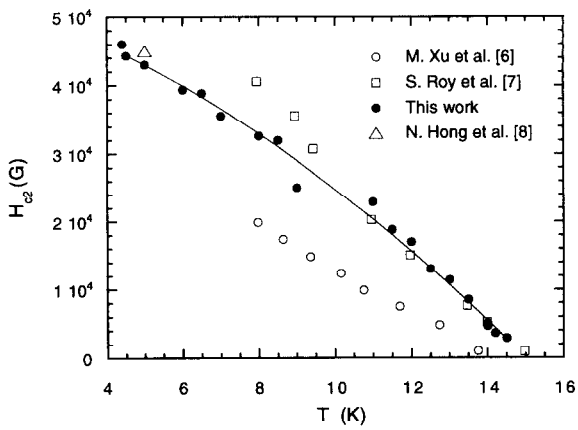

Fig. 7. Comparison of $H_{c2}(T)$ obtained by different groups.

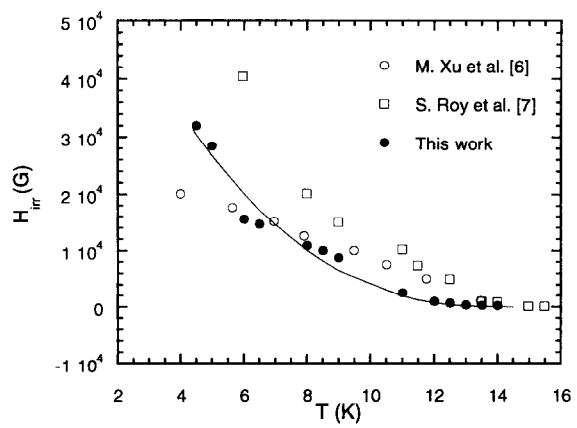

Fig. 8. Comparison of $H_{c1}(T)$ obtained by different groups.

$$F_p = \frac{1}{c} |j_c \times B| , \quad (4)$$

which directly characterizes the interaction between the vortices and the pinning centers. In order to evaluate the pinning force for YNi_2B_2C we derive the critical current density j_c from the irreversible moment M_{irr}. This is done by using the usual Bean model [9] for an ellipse of semiaxes $b=0.5$ cm, $a=0.3$ cm and thickness $t=0.1$ cm for which $j_c=10M_{irr}/a(1-a/3b)$. Here j_c is in A/cm^2, M_{irr} in emu/cm^3 and the lengths are in cm. Typical results, for temperatures $T=4.4$, 6.5 and 8.5 K are shown in Fig. 9. Apparently, the critical current decays very fast with field but, even in the remanent state $j_c \approx 2.5 \times 10^3$ A/cm^2 at $T=4.4$ K, three orders of magnitude less than for high-T_c superconductors. In Fig. 10 we plot the pinning force, evaluated by using Eq. (4). Each of the $F_p(T, H)$ curves exhibits a maximum; the coordinates of the maximum are denoted here as $(H_{max}, F_{p,max})$. In Fig. 11 we plot several curves of the pinning force in the normalized coordinates: $(h=H/H_{max}, f_p=F_p/F_{p,max})$. In these coordinates all the curves collapse on a unique curve. Similar behavior was observed in both conventional [10] and high-T_c [11] materials. We note, however, that the functional form of the curve in Fig. 11 cannot be fitted by the conventional [11] expression $f_p \propto h^p(1-\gamma h)^q$, implying an unusual pinning mechanism in this compound.

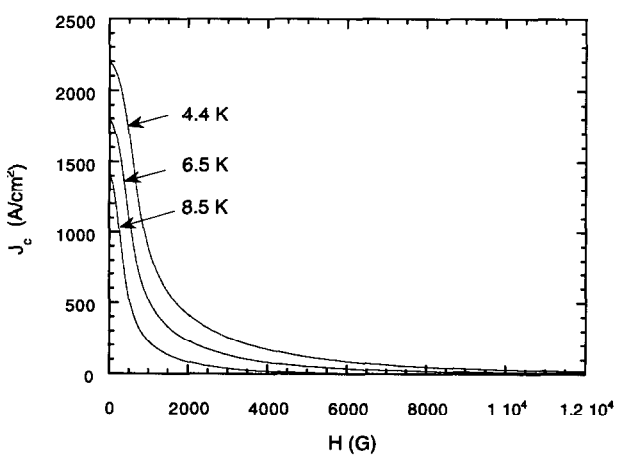

Fig. 9. Critical current density at $T=4.4$, 6.5 and 8.5 K vs. magnetic field.

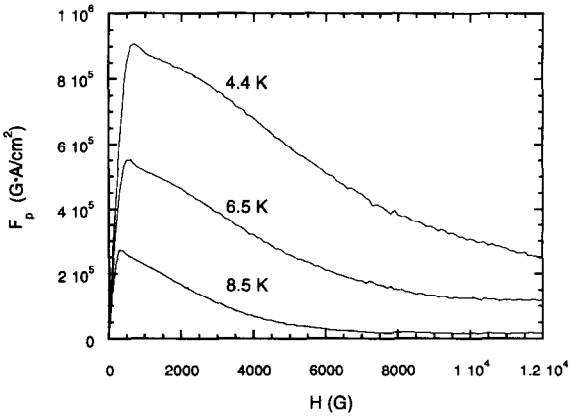

Fig. 10. Pinning force at $T=4.4$, 6.5 and 8.5 K vs. magnetic field

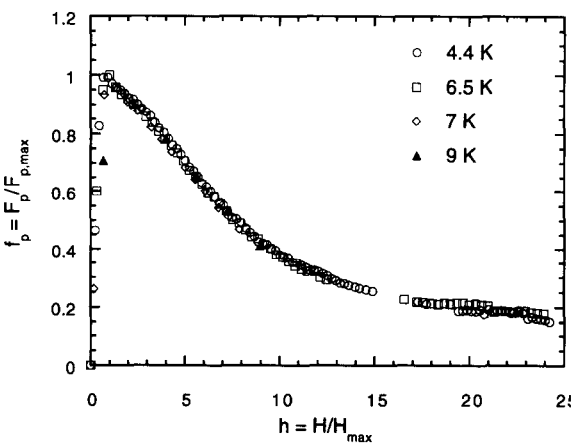

Fig. 11. Scaling of the normalized pinning force.

3.7. Relaxation

For the magnetic relaxation measurements, the sample was zero-field cooled down to a given temperature. Then magnetic field was ramped up in a sweep mode with a rate 500 G/s up to the field of 2000 G. Fig. 12 presents relaxation curves measured on sample #2 at different temperatures. A fast relaxation during the first seconds is followed by a plateau with no noticeable changing in magnetic moment. We find the same behavior for relaxation at different fields for constant temperature. The initial relaxation is best fitted by an exponential dependence in the form $M(t)=M(0)\,e^{t/t_0}+M(\infty)$. Typical fits are shown in the inset to Fig. 8. The best values for t_0 are presented in Fig. 13. The solid line in the figure is a fit to

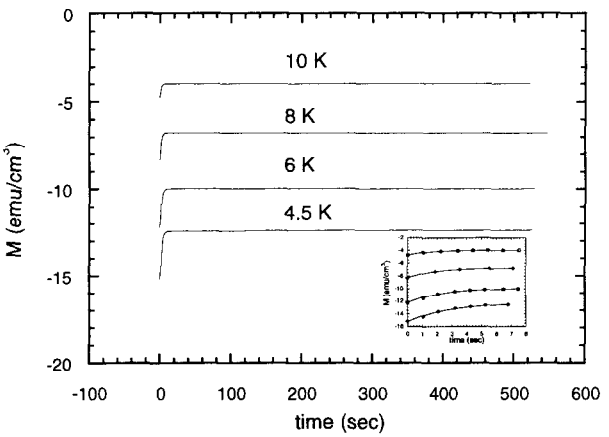

Fig. 12. Magnetic relaxation measured by VSM at $T=4.5$, 6, 8 and 10 K at $H=2000$ G. (Inset) blow-up of the short-time relaxation showing exponential fit (see text).

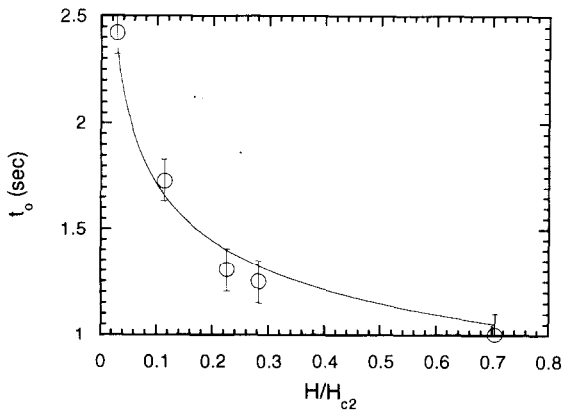

Fig. 13. The relaxation constant ($T=7$ K) as a function of the external magnetic field.

$t_0 \approx 0.96/(H/H_{c2})^{1/4}$. This unusual behavior calls for further study.

4. Summary

We have presented detailed magnetic measurements performed on the recently discovered YNi_2B_2C superconductor. Table 1 summarizes all the characteristic parameters that we have found in our study. In general, we find that the magnetic behavior of this compound is very similar, at least quantitatively, to that of type-II conventional superconductors with weak pinning centers.

Table 1

$H_{c1}(T) \approx 83.4[1-(T/T_c)^2]$ G
$H_{c2}(T) \approx 47600[1-(T/T_c)^2]$ G
$\lambda(T) \approx (3.5\times10^{-5})\sqrt{1-(T/T_c)^4}$ cm
$\xi(T) \approx 10^{-6}\sqrt{1-(T/T_c)^4}$ cm
$\kappa \approx 35 \pm 3$
$H_{irr}(T) \approx 81000(1-T/T_c)^{2.7}$ G
$j_c(T=4.4\text{ K}, H=0) \approx 2.5\times10^3$ A/cm^2

Acknowledgement

We thank John Clem for a critical reading of the manuscript and corrections to Eqs. (1a) and (2). This research was supported in part by the Israeli Ministry of Sciences and Art and in part by the Klachky Foundation for Superconductivity.

References

[1] J.R. Gavaler, M. Janocko and C.J. Jones, J. Appl. Phys. 49 (1974) 3009.
[2] C. Mazumdar, R. Nagarajan, C. Godart, L.C. Gupta, M. Latroche, S.K. Dhar, C. Levy-Clement, B.D. Padalia and R. Vijayaraghavan, Solid State Commun. 87 (1993) 413.
[3] R. Nagarajan, C. Mazumdar, Z. Hossain, S.K. Dhar, K.V. Gopalakrishnan, L.C. Gupta, C. Godart, B.D. Padalia and R. Vijayaraghavan, Phys. Rev. Lett. 72 (1994) 274.
[4] R.J. Cava, H. Takagi, H.W. Zandbergen, J.J. Krajewski, W.F. Jr. Peck, T. Siegrist, B. Batlogg, R.B. van Dover, R.J. Feder, K. Mizuhashi, J.O. Lee, H. Eisaki and S. Uchida, Nature 367 (1994) 252;
T. Siegrist, H.W. Zandbergen, R.J. Cava, J.J. Krajewski and W.F. Peck, Nature 367 (1994) 254.
[5] I. Felner, Phys. Rev. Lett. 72 (1994) 3742.
[6] M. Xu, P.C. Canfield, J.E. Ostenson, D.K. Finnemore, B.K. Cho, Z.R. Wang and D.C. Johnston, Physica C 227 (1994) 321, submitted.
[7] S.B. Roy, Z. Hossain, A.K. Pradhan, C. Mazumdar, P. Chaddah, R. Nagarajan, C. Godart and L.C. Gupta, Physica C 228 (1994) 319.
[8] N.M. Hong, H. Michor, M. Vybornov, T. Holubar, P. Hundegger, W. Perthold, G. Hilscher and P. Rogl, Physica C 227 (1994) 85.
[9] M. Tinkham, Introduction to Superconductivity (McGraw-Hill, New York, 1975).
[10] C. Hu, Phys. Rev. B 6 (1972) 1756; J.R. Clem, J. Low Temp. Phys. 18 (1975) 427, and private communication.
[11] D. Dew-Hughes, Phil. Mag. 30 (1974) 293; L. Niel, Cryogenics 32 (1992) 975.